

High-energy neutrino fluxes and flavor ratio in the Earth atmosphere

T.S. Sinegovskaya¹, A.D. Morozova² and S.I. Sinegovsky^{3*}

¹ *Irkutsk State Railway University, 664074 Irkutsk, Russia*

² *Physics Faculty, Irkutsk State University, 664003 Irkutsk, Russia*

³ *Institute of Applied Physics, Irkutsk State University, 664003 Irkutsk, Russia*

We calculate the atmospheric neutrino fluxes in the energy range 100 GeV – 10 PeV with usage of several known hadronic models and few parametrizations of the cosmic ray spectra which take into account the knee. The calculations are compared with the atmospheric neutrino measurements by Frejus, AMANDA, IceCube and ANTARES. An analytic description is presented for the zenith-angle averaged conventional ($\nu_\mu + \bar{\nu}_\mu$) and ($\nu_e + \bar{\nu}_e$) energy spectra, which can be used to obtain test data of the neutrino event reconstruction in neutrino telescopes. The sum of the calculated atmospheric ν_μ flux and the IceCube best-fit astrophysical flux gives the evidently higher flux as compared to the IceCube59 data, giving rise the question concerning the hypothesis of the equal flavor composition of the high-energy astrophysical neutrino flux. Calculations show that the transition from the atmospheric electron neutrino flux to the predominance of the astrophysical neutrinos occurs probably at 30 – 100 TeV, if the prompt neutrino component is taken into consideration. The neutrino flavor ratio, extracted from the IceCube data, does not reveal a trend to rise as it is expected for the conventional neutrino flux in the energy range 100 GeV – 30 TeV. A depression of the ratio R_{ν_μ/ν_e} probably indicates that the atmospheric electron neutrino flux obtained in the IceCube experiment contains an admixture of the astrophysical neutrinos in the range 10 – 50 TeV.

PACS numbers: 13.85.Tp, 95.85.Ry, 95.55.Vj

I. INTRODUCTION

High-energy neutrinos produced in decays of pions, kaons, and charmed particles of the extensive air shower induced by cosmic rays passing through the Earth atmosphere, form an unavoidable background for the detection of astrophysical neutrinos. Search of extraterrestrial neutrino sources is the challenge to resolve which large-scale neutrino telescopes, NT200+ [1], IceCube [2–4], ANTARES [5, 6] are designed. The high-energy atmospheric neutrinos became accessible to the experimental studies only last years. By now, the energy spectrum of high-energy atmospheric muon neutrinos has been measured in the four experiments: Frejus [7] at energies up to 1 TeV, AMANDA-II [8] in the energy range 1 – 100 TeV, IceCube [2] at 100 GeV – 400 TeV, and ANTARES at energies 100 GeV – 200 TeV [5]. Not long ago the IceCube presented also results for the electron neutrino spectrum measured in the energy range ~ 80 GeV – 6 TeV [9]. Thus a possibility appeared to evaluate the neutrino flavor ratio using the IceCube measurements and to compare this one with predictions.

Lately IceCube found the 37 high-energy neutrino events [10–12] in energy range 30 TeV - 2 PeV, most of which are hardly consistent with events expected from the atmospheric muons and neutrinos, 8.4 ± 4.2 and $6.6_{-1.6}^{+5.9}$ respectively. The neutrino events, three of which have energies above 1 PeV were detected over the three years 2010-2013 (988 days), give the statistical significance of their astrophysical origin at the level of 5.7σ .

After the IceCube reported [10] on the detection of the first two neutrino-induced events with deposited energy 1.04 and 1.14 PeV, the prompt analysis of the origin of the highest energy neutrinos ever detected was performed [13–15].

Increasing with energy contribution of charmed particles to the atmospheric neutrino flux becomes the source of the large uncertainty at energies above ~ 200 TeV for muon neutrinos, and above ~ 20 TeV for electron neutrinos. More complicated picture is likely if the astrophysical neutrinos and the atmospheric conventional/prompt ones are entangled. It is quite possible that astrophysical neutrino flux becomes dominant over the atmospheric electron neutrino flux at energies 20 – 50 TeV. Thus a comparison of atmospheric neutrino spectra calculated for various hadron-interaction models with high-energy neutrino spectra measurements can shed light on the most uncertain constituent of the atmospheric neutrino background, in spite of large statistical and systematic uncertainties.

Here we calculate atmospheric neutrino fluxes at energies $10^2 - 10^7$ GeV for zenith angles from 0° to 90° as well as the angle averaged spectrum with the use of high-energy hadronic interaction models QGSJET II-03 [16] and SIBYLL 2.1 [17]. These models are widely employed to simulate extensive air showers (EAS) with the Monte Carlo method, and were also applied to compute the cosmic-ray hadron and muon fluxes [18, 19]. Besides, in this work computation, we employ also the known old hadronic model by Kimel & Mokhov (KM) [20] which was checked by comparison of the calculated atmospheric hadron and muon spectra with the experiment [18].

The calculation has been performed for three parametrizations of the measured spectrum and the com-

* E-mail: sinegovsky@api.isu.ru

position of primary cosmic rays in the energy range comprising the knee: 1) the model by Zatsepin & Sokolskaya (ZS) [21] include only Galaxy sources, 2) the model by Hillas [22] and Gaisser (HGm) [23], and 3) the modified multi-knee (polygonato) model (BK) [24, 25]. Below we denote for short different versions of the calculations according to the pattern “a primary cosmic ray spectrum + a hadronic interaction model” or vice versa, “a hadronic interaction model + a primary cosmic ray spectrum”. For example: HGm+QGSJET (or HGm+QGS2), ZS+QGS2, HGm+KM, SIBYLL+BK, and so on.

The paper is organized as follows. In Sec. II we give a sketch of the computation scheme: a short review of the calculation method and the data input, primary cosmic-ray spectra and hadronic interaction models used in the computation. In Sec. III presented are the results of calculation of the atmospheric muon neutrino energy spectrum and comparison with experiments. In Sec. IV we compare calculations of the electron neutrino spectrum and the neutrino flavor ratio R_{ν_μ/ν_e} with IceCube measurements. Main results of the paper are discussed in Sec. V.

II. SCHEME OF THE COMPUTATION

A. Outline of the calculation method

To compute the atmospheric muon and electron neutrino spectra we employ the method to solving the hadron cascade equations [18, 26] that make it possible to account for the non-power behavior of the cosmic-ray spectrum, energy dependent total inelastic cross sections $\sigma_{hA}^{in}(E)$ of hadron-nucleus interactions, and a violation of Feynman scaling law for the inclusive cross sections. The calculation procedure was validated through the careful comparison with experiments of the calculated atmospheric hadron fluxes and the sea-level muon spectrum which covers the wide energy range for different zenith angles [18, 19]. Omitting details we give here a brief review of the calculation scheme aimed to introduce generalized Z -factors.

The differential energy spectra of the secondary protons $p(E, h)$ and neutrons $n(E, h)$ at atmospheric depth h obey the equations

$$\frac{\partial N^\pm(E, h)}{\partial h} = -\frac{N^\pm(E, h)}{\lambda_N(E)} + \frac{1}{\lambda_N(E)} \times \int_0^1 \Phi_{NN}^\pm(E, x) N^\pm(E/x, h) \frac{dx}{x^2}, \quad (1)$$

where $N^\pm(E, h) = p(E, h) \pm n(E, h)$,

$$\Phi_{NN}^\pm(E, x) = \frac{E}{\sigma_{pA}^{in}(E)} \left[\frac{d\sigma_{pp}(E_0, E)}{dE} \pm \frac{d\sigma_{pn}(E_0, E)}{dE} \right],$$

$\lambda_N(E) = [N_0 \sigma_{pA}^{in}(E)]^{-1}$ is the nucleon interaction length, $N_0 = N_A/A$ is the number of nuclei per gram of

air, $x = E/E_0$ is the fraction of the primary nucleon energy E_0 carried away by the secondary nucleon, $d\sigma_{ab}/dE$ is a cross section for the inclusive reaction $a + A \rightarrow b + X$, integrated over the transverse momentum. The boundary conditions for Eq. (1) are: $N^\pm(E, 0) = p_0(E) \pm n_0(E)$.

Let us seek a solution of system (1) in the form

$$N^\pm(E, h) = N^\pm(E, 0) \exp \left[-\frac{h(1 - \mathcal{Z}_{NN}^\pm(E, h))}{\lambda_N(E)} \right], \quad (2)$$

where $\mathcal{Z}_{NN}^\pm(E, h)$ are unknown functions. Substitution of Eq. (2) into (1) yields equations for the functions \mathcal{Z}_{NN}^\pm (\mathcal{Z} -factors):

$$\frac{\partial(h\mathcal{Z}_{NN}^\pm)}{\partial h} = \int_0^1 dx \Phi_{NN}^\pm(E, x) \eta_{NN}^\pm(E, x) \times \exp[-h\mathcal{D}_{NN}^\pm(E, x, h)], \quad (3)$$

where $\eta_{NN}^\pm(E, x) = x^{-2}N^\pm(E/x, 0)/N^\pm(E, 0)$,

$$\mathcal{D}_{NN}^\pm(E, x, h) = \frac{1 - \mathcal{Z}_{NN}^\pm(E/x, h)}{\lambda_N(E/x)} - \frac{1 - \mathcal{Z}_{NN}^\pm(E, h)}{\lambda_N(E)}. \quad (4)$$

Integrating Eq. (3), one obtains a nonlinear integral equation,

$$\mathcal{Z}_{NN}^\pm(E, h) = \frac{1}{h} \int_0^h dt \int_0^1 dx \Phi_{NN}^\pm(E, x) \eta_{NN}^\pm(E, x) \times \exp[-t\mathcal{D}_{NN}^\pm(E, x, t)], \quad (5)$$

which we solve using the iterative approach. Choosing as the starting point $\mathcal{Z}_{NN}^{\pm(0)}(E, h) = 0$, i.e. $\mathcal{D}_{NN}^{\pm(0)}(E, x, h) = 1/\lambda_N(E/x) - 1/\lambda_N(E)$, we find for the n -th step

$$\mathcal{Z}_{NN}^{\pm(n)}(E, h) = \frac{1}{h} \int_0^h dt \int_0^1 dx \Phi_{NN}^\pm(E, x) \eta_{NN}^\pm(E, x) \times \exp[-t\mathcal{D}_{NN}^{\pm(n-1)}(E, x, t)], \quad (6)$$

$$\mathcal{Z}_{NN}^{\pm(n)}(E, h) = \frac{1}{h} \int_0^h dt \int_0^1 dx \Phi_{NN}^\pm(E, x) \eta_{NN}^\pm(E, x) \times \exp[-t\mathcal{D}_{NN}^{\pm(n-1)}(E, x, t)], \quad (7)$$

where

$$\mathcal{D}_{NN}^{\pm(n-1)}(E, x, h) = \frac{1 - \mathcal{Z}_{NN}^{\pm(n-1)}(E/x, h)}{\lambda_N(E/x)} - \frac{1 - \mathcal{Z}_{NN}^{\pm(n-1)}(E, h)}{\lambda_N(E)}. \quad (8)$$

The functions $\mathcal{Z}(E, h)$ depend on two variables unlike the commonly known z -factor and carry imprints of cosmic ray spectra, hadron-nuclei interactions and the hadronic cascade evolution in the atmosphere. In the case of the power-law cosmic ray spectrum, the Feynman scaling for the hadron production cross sections and $\sigma_{hA}^{in} = \text{const}$ functions $\mathcal{Z}_{ab}(E, h)$ reduce to constants or $z_{ab}(E)$ (see details in Refs. [19, 27])

In similar fashion meson cascade equations can be solved having the nucleon and meson sources [18]. The main pion sources in the atmospheric shower are the interactions of nucleons and pions with air nuclei and kaon decays. At the first step, the meson component can be detached from the nucleon one by neglecting the small contribution from the $N\bar{N}$ pair production in meson–nucleus collisions. Specifically, pion equations are detached from the kaon ones if at first to neglect decays of kaons to pions, and the pion production by kaons. In turn, the kaon part of cascade contains the nucleon source as the main one and pion sources as additional source inasmuch as the reaction $\pi + A \rightarrow K + X$ taking into account.

After the first step calculation of nucleon and meson fluxes one can calculate small corrections to the nucleon, pion and kaon fluxes: (i) account the additional pion source from decays of kaons to pions; (ii) account for $K + A \rightarrow \pi + X$; (iii) account for $N\bar{N}$ pair production.

The Genz-Malik adaptive cubature algorithm [28] turned out to be very useful in a numerical realization of the method for multidimensional integration; a fast algorithm based on quadratic B-splines was used to interpolate and approximate the calculated functions. Note the high convergence of the method: in the nucleon component calculations, five iterations are required to achieve an accuracy close to 1%, while two iterations are enough to achieve the same accuracy in the meson flux computations.

B. Primary cosmic-ray spectra

As the primary cosmic ray spectra and composition in wide energy range we use in our calculations following models: 1) the model by Zatsepin & Sokolskaya (ZS), 2) the novel CR approximation (HGm) by Hillas [22] and Gaisser [23], and 3) the modified multi-knee model by Bindig, Bleve and Kampert (BK) [24] based on KASCADE data [29] and the polygonato model by Hörandel [25].

The Zatsepin and Sokolskaya model [21] comprises contributions to the cosmic ray flux of three classes of Galaxy astrophysical sources : (I) isolated (non associated) SNe exploding into random interstellar medium (ISM) (the magnetic rigidity $R = E_{\text{CR}}/eZ < 50$ TV); (II) the most powerful sources of CR are high mass supernovae (SNe) exploding into ISM in OB associations which give rise particles with energies up to $4Z$ PeV: CR particles are accelerated by shock waves passing through the stellar wind, i.e. OB star explodes into a dense ISM ($R < 4$ PV); (III) the weak sources include explosions of novae ($R < 200$ GV).

All of three classes of CR sources produce power-law energy spectra with different spectral indices $\gamma = \alpha + 0.33$, where α is the index of source spectrum. In the region of effective acceleration spectral indices are 2.63 (class I), 2.43 (II), 2.90 (III). For the energies range $E = 100$ TeV - 1 PeV: the rise of p, He ($\gamma_{\text{p,He}} < 2.75$); the fall

of median nuclei (CNO) and heavy ones ($\gamma_{\text{CNO}} > 2.75$). For $E > 3$ PeV (above the knee): p, He diminish, heavy nuclei grow. For $E > 30$ PeV Fe dominates.

The model ZS describes well data of the ATIC2 direct measurements [30] in the range $10 - 10^5$ GeV and gives a motivated extrapolation of these data up to 100 PeV – the energy region where the cosmic ray spectra and elemental composition are derived from measured characteristics of EAS. The ZS proton spectrum at $E \gtrsim 10^6$ GeV is compatible with KASCADE data as well the helium one within the range of the KASCADE spectrum obtained with the usage of hadronic models QGSJET01 and SIBYLL, and well agree with the Hillas-Gaisser model up to 1 PeV.

Since direct measurements of the cosmic ray spectra and elemental composition are terminated close to 100 TeV, one needs to make the spectrum extrapolation to high energies, above the knee. The model by Hillas and Gaisser [22, 23] includes three classes of sources: i) supernova remnants in the Galaxy, ii) Galaxy high-energy sources of still uncertain origin which contribute to the cosmic ray flux between the “knee” (3 PeV) and the “ankle” (4 EeV), iii) extragalactic astrophysical objects (Active Galactic Nuclei, sources of the Gamma-Ray Bursts and others).

The composite spectrum is formed of five groups of nuclei (p, He, CNO, Mg-Si and Mn-Fe). Each of the three populations accelerates five groups of nuclei, the spectrum of which cuts off at a characteristic rigidity. The parameters for the class 1 spectrum were taken from CREAM measurements [31] and extrapolated (to a rigidity of 4 PV) to take into account the knee. The extrapolation is consistent with measurements of the all-particle spectrum beyond the knee in the EAS experiments. The extragalactic component takes into account also the measurement data by HiRes, PAO and Telescope Array. In our calculations, we use the version with mixed composition for extragalactic sources of cosmic rays, denoted here as HGm, which corresponds to the H3a of Ref. [32]). More details concerning this parametrization one can find also in Ref. [33].

Polygonato model [25] comprising only galactic sources is third known cosmic-ray model used in our calculations. The modified multi-knee (polygonato) model by Bindig, Bleve and Kampert [24] was aimed to take into account the KASCADE data [29] concerning elemental composition of cosmic rays around the knee.

C. High-energy hadronic interaction models

Calculations of hadronic cascades induced by high-energy cosmic-ray particles and the atmospheric neutrino flux of the PeV scale require either an extrapolating cross sections measured at lower energies or developing the models to give the reliable predictions at high and ultrahigh energies. Direct measurements of inclusive cross sections for the nucleon and meson production in hadron-

nucleus collisions are still far from being complete because of the restricted kinematics region of LHC cross section measurements.

In this work, we apply known hadronic interaction models QGSJET II-03 [16], SIBYLL 2.1 [17] currently undergoing overall test in two ways: (i) simulations of EAS, induced by high-energy cosmic-ray particles and (ii) through comparison of the model predictions with results of LHC experiments.

Besides we use also the hadronic interaction model proposed by Kimel and Mokhov (KM) [20], for which we adopt updated parameters [26, 34, 35]. Based on accelerator data at energies up to 1.5 TeV, KM however obeys the Feynman scaling law and can be valid for higher energies making predictions compatible with QGSJET and SIBYLL. The predictions of KM model for pp and pA interactions are also close to results obtained in hadronic model DPMJET-III [36, 37] based (like SIBYLL) on the dual parton model. The KM model was also applied in 3D Monte Carlo calculations of the atmospheric neutrino fluxes [38].

The current models differ in accuracy of description of soft interactions and contribution of the diffraction dissociation, in ways to account for semihard interactions (minijets), in description of hadron-nucleus interactions (Glauber approach or Glauber-Gribov theory, semisuperposition or superposition picture), in the degree of the scaling violation at high energies.

To illustrate in part the difference of the hadronic models one can compute the cosmic ray spectrum-weighted moments (z -factors) for proton-air interactions $pA \rightarrow cX$ of the inclusive spectra $(x/\sigma_{pA}^{in})(d\sigma_{pc}/dx)$:

$$z_{pc}(E_0) = \int_0^1 \frac{x^\gamma}{\sigma_{pA}^{in}} \frac{d\sigma_{pc}}{dx} dx, \quad (9)$$

where $x = E_c/E_0$, $\gamma = 1.7$, $c = \pi^\pm, K^\pm$; z -factors for DPMJET-III are borrowed from Ref. [37] (see [36]). As one can see from Tab. I, z -factors obey the approximate

TABLE I. z_{pc} -factors for π and K mesons.

Model	E_0 , GeV	$z_{p\pi^+}$	$z_{p\pi^-}$	z_{pK^+}	z_{pK^-}
QGSJET	10^2	0.043	0.035	0.0036	0.0030
	10^3	0.036	0.029	0.0036	0.0028
II-03	10^4	0.033	0.028	0.0034	0.0027
SIBYLL	10^2	0.036	0.026	0.0134	0.0014
	10^3	0.038	0.029	0.0120	0.0023
2.1	10^4	0.037	0.029	0.0097	0.0027
KM	10^2	0.044	0.027	0.0051	0.0015
	10^3	0.046	0.028	0.0052	0.0015
	10^4	0.046	0.029	0.0052	0.0015
DPMJET	10^3	0.04	0.035	0.0070	0.0035
	III	10^4	0.04	0.035	0.0070

scaling law in DPMJET-III, KM and SIBYLL 2.1 (but the production of K -mesons), while in case of QGSJET-II noticeable violation of the scaling is found just for pions.

III. FLUXES OF ATMOSPHERIC MUON NEUTRINOS

The calculation is performed on the basis of the method [26] of solution of the hadronic cascade equations in the atmosphere, which allows us to describe the hadron-nucleus cascade induced by cosmic rays in air taking into the non power law energy spectrum of the primary cosmic rays, the violation of Feynman scaling, and the growth of the total inelastic cross sections for hadron-nucleus collisions with increasing energy (see also [18]). Along with major sources of the muon neutrinos, $\pi_{\mu 2}$ and $K_{\mu 2}$ decays, we consider three-particle semileptonic decays, $K_{\mu 3}^\pm$ (the branching ratio 3.32%), $K_{\mu 3}^0$ (27%), the contribution originated from decay chains $K \rightarrow \pi \rightarrow \nu_\mu$ ($K_S^0 \rightarrow \pi^+\pi^-, K^\pm \rightarrow \pi^\pm\pi^0$), as well as small fraction from the muon decays.

The comparison of the muon neutrino fluxes calculated with three recent primary spectrum models (Fig. 1) shows that they are rather close each other up to 1 PeV. In Tab. II presented are neutrino flux ratios (averaged over zenith angles) calculated with usage of three hadronic models QGSJET-II, SIBYLL and KM: columns marked as 1, 2, 3 present comparative ($\nu_\mu + \bar{\nu}_\mu$) fluxes, $\phi_{\nu_\mu}^{(SIBYLL)}/\phi_{\nu_\mu}^{(QGSJET\ II)}$, $\phi_{\nu_\mu}^{(KM)}/\phi_{\nu_\mu}^{(QGSJET\ II)}$, and $\phi_{\nu_\mu}^{(SIBYLL)}/\phi_{\nu_\mu}^{(KM)}$ respectively. Columns 4, 5, 6 give the same for the conventional $\nu_e + \bar{\nu}_e$ flux. All computations are performed for ZS and HGm cosmic ray spectra. One

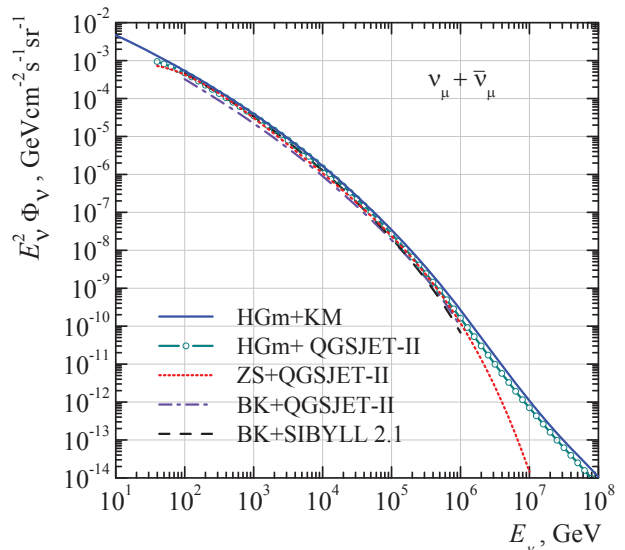


FIG. 1. Comparison of atmospheric $\nu_\mu + \bar{\nu}_\mu$ fluxes calculated using three hadronic models, KM, QGSJET-II-03, SIBYLL 2.1, and three parametrizations of the cosmic-ray spectrum.

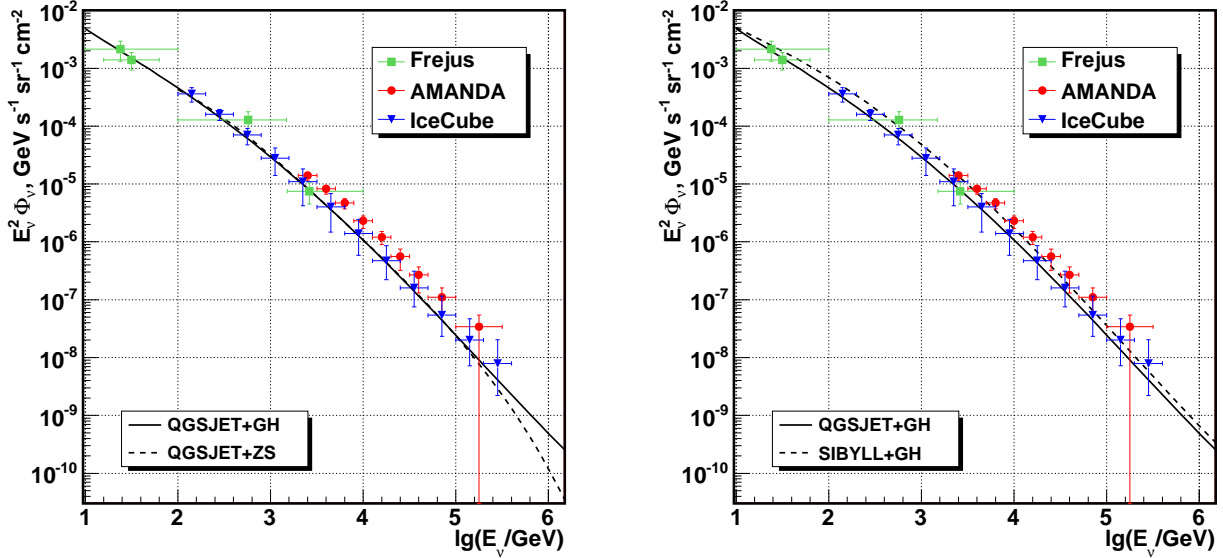


FIG. 2. Conventional $\nu_\mu + \bar{\nu}_\mu$ spectrum averaged over zenith angles: a dependence on the cosmic ray spectrum (left panel) and the hadronic model (right). Symbols: data of Frejus [7], AMANDA-II [8] and IceCube [2] experiments.

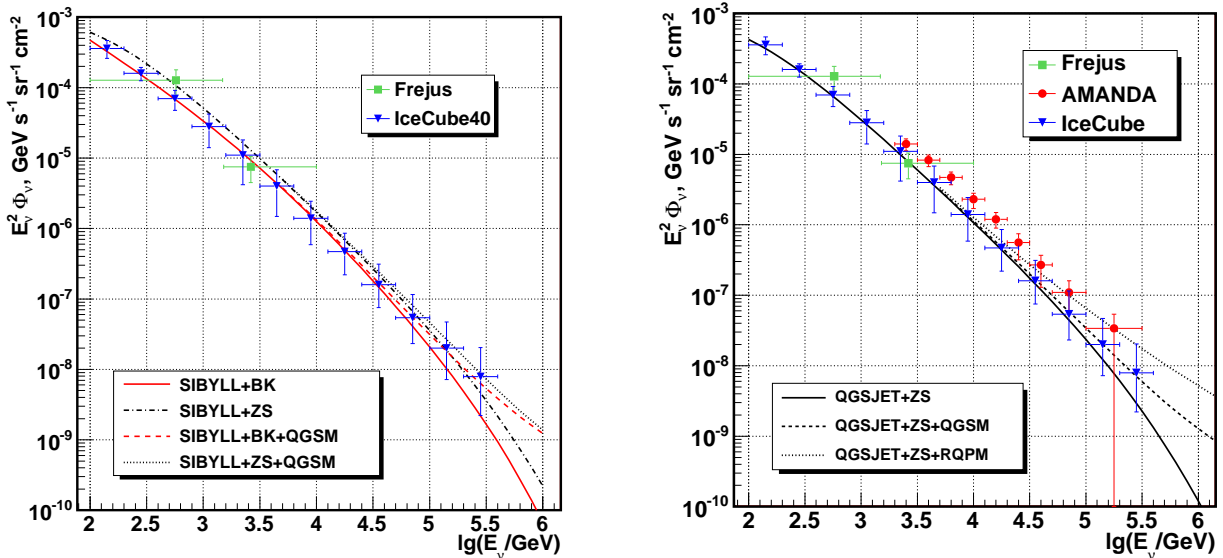


FIG. 3. Fluxes of the conventional and prompt (QGSM, RQPM) muon neutrinos ($\nu_\mu + \bar{\nu}_\mu$) calculated with usage of SIBYLL 2.1 (left panel) and QGSJET II (right panel) for the cosmic-ray spectrum parametrizations involving the knee.

can see that QGSJET-II and SIBYLL 2.1 lead to apparent difference in the muon neutrino flux, as well as in the case of SIBYLL as compared to KM. However with the energy rise the flux difference between SIBYLL and KM predictions diminishes, so that at energies above 100 TeV these fluxes are in close agreement. Quite contrary, the QGSJET-II and KM flux difference becomes notable just above 100 TeV.

In Figs. 2, 3, the conventional $\nu_\mu + \bar{\nu}_\mu$ flux averaged

over zenith angles in the range $96^\circ - 180^\circ$ (the upward neutrinos, $\cos\theta \lesssim -0.1$), calculated with use of ZS and BK spectra are compared with Frejus [7], AMANDA-II [8], and IceCube40 [2] measurement data obtained with the 40-string configuration of the IceCube detector.

To illustrate the influence of the “knee” in the cosmic ray spectrum, in Fig. 2 we plotted also the conventional ($\nu_\mu + \bar{\nu}_\mu$) spectrum computed with usage of the cosmic ray parametrization by Gaisser, Honda, Lipari and Stanev

TABLE II. The neutrino flux ratio calculated with SIBYLL 2.1, QGSJET II-03 and KM for cosmic ray spectra ZS [21] and HGm [23]: sib/qgs2 – column 1 (4); km/qgs2 – 2 (5); sib/km – 3 (6).

E_ν , GeV	1	2	3	4	5	6
	ZS: $(\nu_\mu + \bar{\nu}_\mu)$			ZS: $(\nu_e + \bar{\nu}_e)$		
10^3	1.70	1.05	1.62	1.48	0.85	1.74
10^4	1.53	1.04	1.47	1.39	0.81	1.72
10^5	1.53	1.10	1.39	1.35	0.95	1.42
10^6	1.79	1.64	1.09	1.48	1.56	0.96
10^7	1.85	2.08	0.89	1.45	1.91	0.76
	HGm: $(\nu_\mu + \bar{\nu}_\mu)$			HGm: $(\nu_e + \bar{\nu}_e)$		
10^3	1.59	0.85	1.87	1.45	0.81	1.79
10^4	1.57	1.12	1.40	1.41	0.85	1.65
10^5	1.57	1.27	1.24	1.38	1.01	1.37
10^6	1.63	1.63	1.00	1.37	1.27	1.08
10^7	1.47	1.53	0.96	1.28	1.10	1.17

(GH) [39]. The right panel of Fig. 2 shows an influence of the hadronic models, QGSJET vs. SIBYLL (see also Tab. II). The difference in the neutrino flux predictions resulted from cosmic ray spectra becomes apparent at high neutrino energies: the flux obtained for GH spectrum at 600 TeV is nearly twice as large as that for ZS spectrum for the same hadronic model. Close to 1 PeV this discrepancy increases to the factor five. More results concerning the muon neutrino calculations compared to the AMANDA and IceCube40 measurements were presented in Refs. [40–42].

The prompt neutrino flux was calculated using the quark-gluon string model (QGSM) by Kaidalov & Piskunova [43, 44] as well as the recombination quark-parton model (RQPM) [44]. In Fig. 3 the prompt neutrino calculations were performed with the parametrization of cosmic ray spectrum by Nikolsky, Stamenov and Ushev (NSU) [45], therefore they can serve here as upper limits for the prompt neutrino flux due to QGSM or RQPM.

Addition of the QGSM prompt contribution evidently improves the agreement of the calculation example ZS+QGSJET with the IceCube40 measurement data [2] above 100 TeV. The prompt neutrino flux due to QGSM and RQPM can be approximated at energies $5 \text{ TeV} \leq E \leq 5 \text{ PeV}$ by the expressions

$$\phi_\nu^{(\text{qgsm})}(E) = A(E/E_1)^{-3.01}[1 + (E/E_1)^{-2.01}]^{-0.165}, \quad (10)$$

$$\phi_\nu^{(\text{rqpm})}(E) = B(E/E_1)^{-2.96}[1 + (E/E_1)^{-1.96}]^{-0.157}, \quad (11)$$

where $A = 1.19 \cdot 10^{-18}$, $B = 4.65 \cdot 10^{-18} (\text{GeV cm}^2 \text{ s sr})^{-1}$, $E_1 = 100 \text{ TeV}$.

Figure 4 shows calculations of the atmospheric muon neutrino spectrum in comparison with the measurement data obtained in recent experiments, IceCube40 [2],

ANTARES [5] and IceCube59 [46]. In Ref. [46] results were presented of the novel reconstruction of the muon neutrino spectrum with use of the data obtained with the 59-string IceCube configuration. The calculations of the conventional flux were performed for a set of models: HGm+QGSJET-II (red solid line), HGm+SIBYLL (magenta), HGm+KM (blue bold dots), ZS+QGSJET-II (dashed line). The QGSM and RQPM prompt neutrino fluxes obtained [44] with NSU spectrum are shown separately (short dash and dash-dot lines, respectively). The total atmospheric $(\nu_\mu + \bar{\nu}_\mu)$ spectrum was calculated with the model HGm+QGSJET+QGSM (blue solid line).

The conventional flux due to the HGm+QGSJET is similar to that of ZS+QGSJET up to 1 PeV. The difference of the neutrino flux predictions originated from the primary cosmic ray spectra becomes apparent above 1 PeV: the flux obtained with QGSJET-II for ZS spectrum at 2 PeV is less by a third of the flux for HGm spectrum.

The HGm+KM calculation represents in fact a kind of an interpolating flux (between QGSJET-II-03 flux and SIBYLL 2.1 one) because the HGm+KM prediction is in close agreement with HGm+QGSJET one at lower energies and agrees well with HGm+SIBYLL above 100 TeV; the blue bold dot curve and thin magenta one merge into one curve at $E > 200 \text{ TeV}$ (Fig. 4).

Being in a close agreement with the IceCube59 mea-

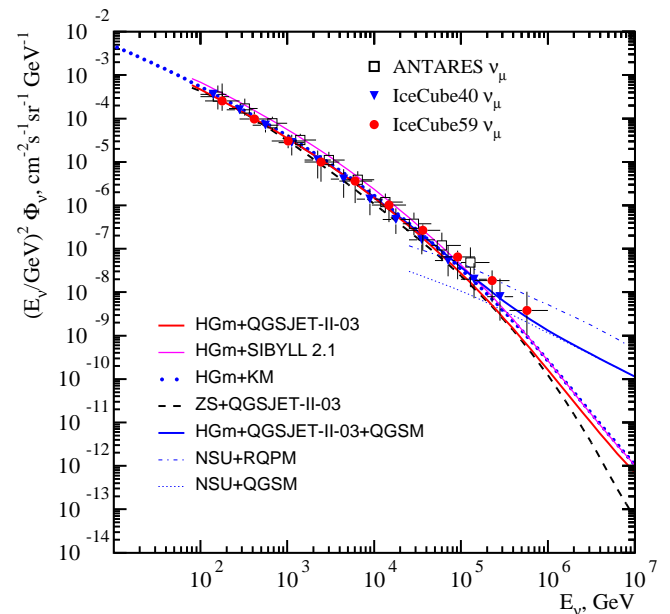


FIG. 4. The atmospheric $\nu_\mu + \bar{\nu}_\mu$ flux calculations versus the experiment. Conventional flux: HGm+QGSJET (red solid line), HGm+SIBYLL (thin magenta), HGm+KM (bold dots), ZS+QGSJET (dashed). Prompt neutrinos (separately): QGSM (short dash curve), RQPM (dash-dot). Total neutrino flux (sum of the prompt flux and conventional one): HGm+QGSJET+QGSM (blue solid line). The measurement data (symbols): IceCube40 [2], IceCube59 [46] and ANTARES [5].

surement data in the energy range from 180 GeV to 36 TeV, the HGm+QGSJET model (only conventional flux) leads to a systematic deviation from the experimental data of the IceCube59 muon neutrino flux, leaving thus the window for the prompt neutrinos. The HGm+QGSJET+QGSM calculation of the total atmospheric ν_μ flux (blue solid line) may be considered as the preferred model, because it describes well the IceCube40 data and gives slightly lowered flux at highest energies reached in IceCube59 experiment. Similar result gives also the HGm+KM+QGSM model.

Note that possible difference of the calculated conventional $\nu_\mu + \bar{\nu}_\mu$ spectrum, resulting from averaging over the zenith angle range $96^\circ - 180^\circ$ (corresponds to the IceCube40 zenith angle cut, $\theta > 97^\circ$ [2]), which differs from the extended range ($\theta > 88^\circ$) in the IceCube59 analysis [46], really does not exceed 13%.

The atmospheric muon neutrino spectrum reconstructed with the IceCube59 data reaches energies above 500 TeV where one expects noticeable admixture of the prompt neutrinos and/or the astrophysical ones. Because the IceCube59 data lead to higher neutrino spectrum (above 10 TeV) as compared to the IceCube40 one, there is no compelling evidence against the QGSM prompt neutrino flux prediction, since HGm+QGSJET-II+QGSM gives the total atmospheric $\nu_\mu + \bar{\nu}_\mu$ flux not exceeding the IceCube59 data at the highest energy ($E_\nu = 575$ TeV) if the IceCube astrophysical flux would be zero.

On contrary, if the prompt neutrino flux would be taken as zero, then adding the best-fit astrophysical flux (Eq. (15), Sect. IV) to the lowest conventional flux prediction (ZS+QGSJET), leads evidently to the higher flux at 575 TeV, $\sim 1.0 \cdot 10^{-8}$ ($\text{GeV cm}^{-2} \text{s}^{-1} \text{sr}^{-1}$), unlike the value $0.38 \cdot 10^{-8}$ in the IceCube59 experiment [46]. Probably, this means that the hypothesis of the flavor equipartition of the IceCube astrophysical neutrino flux ($\nu_e : \nu_\mu : \nu_\tau = 1 : 1 : 1$) is erroneous one [47].

We can describe the conventional zenith-angle averaged $\nu_\mu + \bar{\nu}_\mu$ flux (due to the prediction of the preferred model, HGm+QGSJET-II) by the approximation, valid for $10^2 - 10^7$ GeV with errors not exceed 12% (at lower energies) (in units of $\text{cm}^{-2} \text{s}^{-1} \text{sr}^{-1} \text{GeV}^{-1}$):

$$\lg[E_\nu^2 \phi_{\nu_\mu}^{\pi, K}(E_\nu)] = -(2.31 + 0.198y + 0.165y^2 + 0.00146y^3), \quad (12)$$

where $y = \lg(E_\nu/1 \text{ GeV})$. Here we present also the approximation formula describing our calculation (Sec. IV) for the atmospheric conventional $\nu_e + \bar{\nu}_e$ spectrum (the

TABLE III. Parameters for the conventional neutrino spectra (Eq. (14)).

flavor	C_ν	γ_0	γ_1	γ_2
$\nu_\mu + \bar{\nu}_\mu$	$4.896 \cdot 10^{-3}$	2.198	$1.648 \cdot 10^{-1}$	$1.46 \cdot 10^{-3}$
$\nu_e + \bar{\nu}_e$	$6.053 \cdot 10^{-3}$	2.918	$4.899 \cdot 10^{-2}$	$7.25 \cdot 10^{-3}$

same model, HGm+QGSJET-II-03):

$$\lg[E_\nu^2 \phi_{\nu_e}^{\pi, K}(E_\nu)] = -(2.218 + 0.918y + 0.04899y^2 + 0.00725y^3), \quad (13)$$

Fluxes of neutrinos Eqs. (12), (13) can be rewritten also in the form:

$$\phi_{\nu_e}^{\pi, K}(E_\nu) = C_\nu \left(\frac{E_\nu}{1 \text{ GeV}} \right)^{-(\gamma_0 + \gamma_1 y + \gamma_2 y^2)}. \quad (14)$$

Two sets of the parameters to Eq. (14) are given in Tab. III.

Calculated atmospheric muon neutrino fluxes for the energy range 0.4 – 1 PeV are presented also in Tab. IV along with upper limits on the astrophysical muon neutrino diffuse flux obtained with the ANTARES [6] and IceCube59 [32]. The total atmospheric muon neutrino flux (sum of the conventional flux and prompt one) marked in Tab. IV as “conv. (averaged)+ QGSM” is presented by the preferred model HGm+QGSJET-II + QGSM. Note the prompt neutrino flux obtained with the dipole model (DM) [48] is close to to the QGSM prediction [44] above 1 PeV (about 30% of the disagreement). More intent inspection of the predicted atmospheric neutrino fluxes, both conventional and prompt, shows that distinctions between the DM and QGSM prompt muon

TABLE IV. Atmospheric neutrino flux in the energy range (0.4 – 1) PeV and upper limit for diffuse $\nu_\mu + \bar{\nu}_\mu$ flux obtained with neutrino telescopes.

Model	$E_\nu^2 \phi_\nu$, $\text{GeV (cm}^2 \text{sr)}^{-1}$
conventional $\nu_\mu + \bar{\nu}_\mu$:	$E_\nu = 400 \text{ TeV} - 1 \text{ PeV}$
averaged over angles –	
ZS+SIBYLL 2.1	$(2.21 - 0.214) \times 10^{-9}$
ZS+QGSJET-II	$(1.32 - 0.149) \times 10^{-9}$
BK+QGSJET II	$(1.09 - 0.097) \times 10^{-9}$
HGm+QGSJET II	$(1.45 - 0.163) \times 10^{-9}$
selected zenith angles:	400 TeV - 1 PeV
HGm+QGSJET-II, $\cos \theta = 0.5$	$(0.97 - 0.109) \times 10^{-9}$
HGm+QGSJET-II, $\cos \theta = 0.3$	$(1.56 - 0.176) \times 10^{-9}$
HGm+QGSJET-II, $\cos \theta = 0.1$	$(3.40 - 0.384) \times 10^{-9}$
prompt $\nu_\mu + \bar{\nu}_\mu$:	400 TeV - 1 PeV
NSU+QGSM	$(2.90 - 1.16) \times 10^{-9}$
ZS+QGSM	$(2.23 - 0.54) \times 10^{-9}$
$174E_N^{-3} + \text{DM}$ [48]	$(1.87 - 0.85) \times 10^{-9}$
conv. + prompt $\nu_\mu + \bar{\nu}_\mu$:	400 TeV - 1 PeV
conv.(averaged)+ QGSM	$(4.35 - 1.32) \times 10^{-9}$
conv.(averaged)+ DM	$(3.32 - 1.01) \times 10^{-9}$
conv.($\cos \theta = 0.1$)+QGSM	$(6.30 - 1.54) \times 10^{-9}$
diffuse $\nu_\mu + \bar{\nu}_\mu$:	34.5 TeV - 36.6 PeV
IC59 best fit [32]	0.25×10^{-8}
IC59 limit [32]	1.44×10^{-8}
	45 TeV - 10 PeV
ANTARES limit [6]	4.8×10^{-8}

neutrino flux predictions are hardly observable at the present level of experimental errors, if the knee of the cosmic ray spectrum is thoroughly taken into account.

IV. ELECTRON NEUTRINO FLUX AND THE NEUTRINO FLAVOR RATIO

The sources of the conventional ν_e are three-particle decays of muons μ_{e3} , and kaons K_{e3}^{\pm} , K_{e3}^0 with the branching ratio 5.07% and 40.5% respectively. The latter is dominant source of electron neutrinos at energy below 10 TeV. The semileptonic decays of short-lived K_S^0 also contribute though branching ratio of the decay is small (0.07%) [49]. This decay gives a considerable contribution to the atmospheric ν_e flux at high energies, reaching 36% at $E_\nu = 500$ TeV for zenith angle $\theta = 0^\circ$ (HGm+QGSJET-II model). Close to vertical the $(\nu_e + \bar{\nu}_e)$ flux from the K_S^0 decay becomes nearly equal to that from K_L^0 one at $E_\nu \approx 1$ PeV.

Figure 5 shows zenith-angle dependent ν_e flux ratio, $\phi_\nu(E, \theta)/\phi_\nu(E, 0^\circ)$, calculated for $\theta = 90^\circ$ and 72.5°) with usage of primary spectrum HGm and hadronic interaction models KM, QGSJET-II-03 and SIBYLL 2.1. The curves illustrate partial contributions of the kaon sources varying according to the corresponding critical energy scale depending on zenith angle: $\epsilon_{K_L^0}^{cr}(\theta = 0^\circ) = 210$ GeV, $\epsilon_{K_{e3}^{\pm}}^{cr}(\theta = 0^\circ) = 890$ GeV, $\epsilon_{K_S^0}^{cr}(\theta = 0^\circ) = 120$ TeV (the critical energy for the horizontal is one order of magnitude larger). The “wave” of zenith-angle enhancement

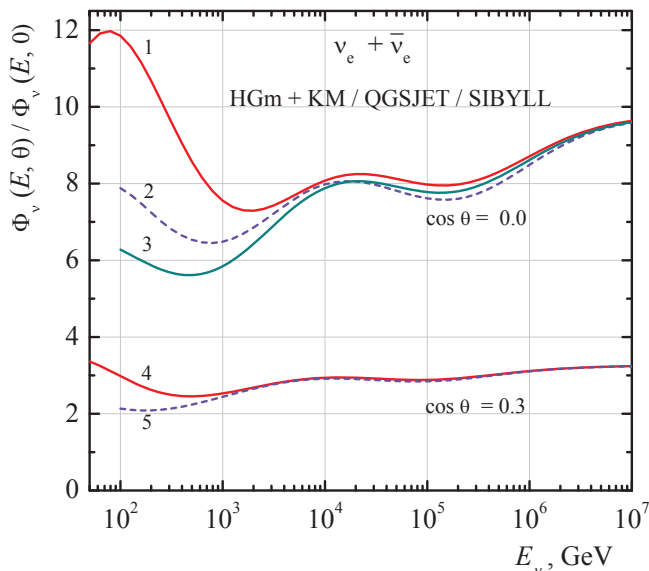


FIG. 5. Zenith-angle enhancement of the atmospheric $(\nu_e + \bar{\nu}_e)$ flux due to energy alignment of the kaon sources. Curves represent the flux ratio, $\phi_{\nu_e}(\theta)/\phi_{\nu_e}(0^\circ)$, calculated with the HGm primary spectrum for 72.5° and $\theta = 90^\circ$: 1 – KM hadronic model (90°), 2 – QGSJET-II-03 (90°), 3 – SIBYLL 2.1 (90°), 4 – KM (72.5°), 5 – QGSJET-II-03 (72.5°).

of the atmospheric $(\nu_e + \bar{\nu}_e)$ flux makes apparent the successive “switching-on” of the kaon sources. The minimum point of the curve reflects the slant neutrino flux maximum (for each of kaon sources) as compared with to vertical. The approximation formula, Eq. (14), describing the calculated zenith-angle averaged energy spectrum of the atmospheric $\nu_e + \bar{\nu}_e$ flux (HGm+QGSJET-II) was given in Sec. III.

Recently the IceCube published results [9] of the first measurement of the atmospheric electron neutrino spectrum in the energy range 80 GeV - 6 TeV obtained with the 79-string IceCube configuration including DeepCore. These measurement data enable to evaluate the neutrino flavor ratio and compare it with predictions.

In Fig. 6 we compare the atmospheric $(\nu_e + \bar{\nu}_e)$ flux calculated using QGSJET II-03 and SIBYLL 2.1 with IceCube measurement data [9] (open triangles) and, besides, with recent IceCube preliminary data for the atmospheric electron neutrinos [51] (red fill triangles).

The diffuse flux of cosmic neutrinos based on 37 events observed in IceCube experiment [11, 12] is presented in Fig. 6) (the green band and red dash-dot line) with use of the IceCube best fits per flavor, $\phi_\nu \sim E^{-2}$ and $\phi_\nu \sim E^{-2.3}$, borrowed from Ref. [12]:

$$E^2 \phi_\nu = (0.95 \pm 0.3) \cdot 10^{-8} \text{ GeV cm}^{-2} \text{ s}^{-1} \text{ sr}^{-1}; \quad (15)$$

$$E^2 \phi_\nu = 1.5 \cdot 10^{-8} (E/100 \text{ TeV})^{-0.3} \text{ GeV}/(\text{cm}^2 \text{ s sr}). \quad (16)$$

In these fits, valid for deposited energies of neutrino events in the range $60 \text{ TeV} < E < 3 \text{ PeV}$, assumed were the flavor ratio $\nu_e : \nu_\mu : \nu_\tau = 1 : 1 : 1$ and zero prompt neutrino flux. The flavor composition of the IceCube astrophysical high-energy neutrino flux is discussed in detail in Refs. [47, 52–55].

The curves in Fig. 6 correspond to calculation results of the atmospheric electron neutrino flux, obtained separately for the conventional neutrinos (HGm/ZS+QGSJET/SIBYLL) and prompt ones due to QGSM. The QGSM prompt neutrino flux represented in Fig. 6 with two curves: green bold dots correspond to the original QGSM flux, Eq. (10), and blue short dash line corresponds to that rescaled with the ZS cosmic ray spectrum. It is clearly seen that the astrophysical ν_e flux and the atmospheric prompt one give competing contributions into detector events at energies above 30 – 50 TeV.

Since IceCube has measured energy spectra both of muon and electron neutrinos, we can try to construct the neutrino flavor ratio $R_{\nu_\mu/\nu_e} = \phi_{\nu_\mu + \bar{\nu}_\mu}/\phi_{\nu_e + \bar{\nu}_e}$ and check for agreement of the calculation with experimental data. The flavor ratio being responsive to changes of the electron neutrino flux, allows one to reveal an admixture of neutrinos from astrophysical sources or small addition of the atmospheric prompt neutrinos.

The difference in atmospheric neutrino flux predictions related to choice of hadronic models is seen in Fig. 7: curves display the scale of difference of the conventional

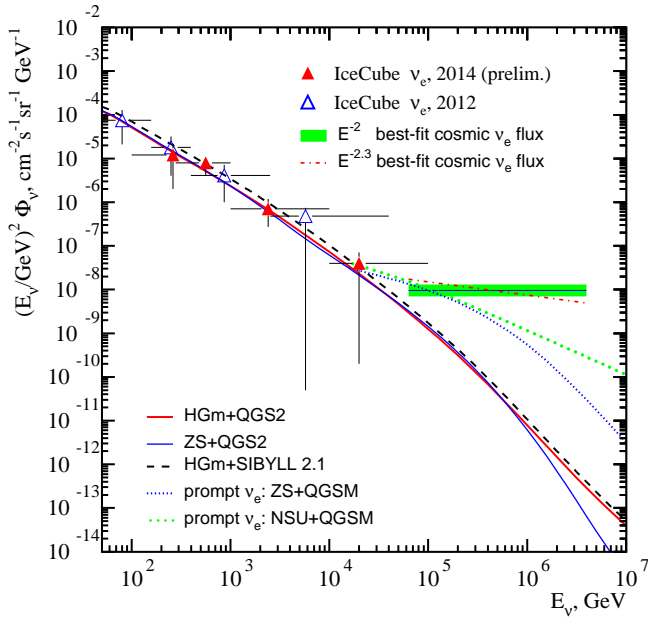


FIG. 6. Atmospheric ($\nu_e + \bar{\nu}_e$) spectrum and the diffuse flux of cosmic neutrinos observed in IceCube experiment [12]. The IceCube measurement of the atmospheric flux of electron neutrinos: [9] (empty triangles) and [51] (filled triangles). Curves: predicted fluxes of the atmospheric conventional and prompt neutrinos. The band width reflects the statistical uncertainty of the IceCube best fit (Eq. (15), see the text), the red dash-dot line corresponds to the second IceCube best fit (Eq. (16)) of the astrophysical neutrino spectrum [12].

neutrino spectra, calculated with models QGSJET-II, SIBYLL 2.1 and KM for HGm and ZS parametrizations of cosmic-ray spectra (HGm+KM/QGSJET/SIBYLL, ZS+QGSJET). The dashed curve (HKKMS, 2007) in Fig. 7 shows the Monte Carlo calculation by Honda et al. [56] done with usage of the hadronic model DPMJET-III [36, 37], the top curve corresponds to R_{ν_μ/ν_e} calculated with KM hadronic model.

This figure displays visible difference of DPMJET-III and KM predictions on the one hand, QGSJET II and SIBYLL on the other, which is partly attributable to the difference of hadronic models in kaon yield (Tab. I). Relative proximity of z -factors for KM and DPMJET-III models leads to similar behavior of the neutrino flavor ratio, R_{ν_μ/ν_e} (Fig. 7). However the R_{ν_μ/ν_e} dissimilarity between SIBYLL and QGSJET-II is not so large as would be expected from the large difference in the kaon production. Contrary, the same model (QGSJET-II) leads also to visible R_{ν_μ/ν_e} distinction because of the cosmic ray spectrum (ZS vs. HGm): HGm+QGSJET-II (curve with dark cyan small squares) and ZS+QGSJET-II (solid red curve).

Relative kaon excess due to KM, DPMJET-III and SIBYLL makes some kind “hierarchy” of the plateau in the energy dependence of R_{ν_μ/ν_e} (still corrected for dif-

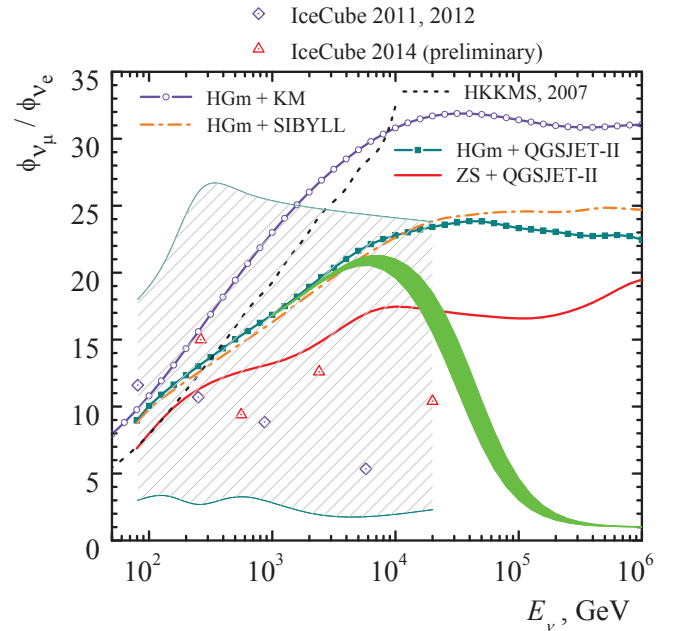


FIG. 7. The atmospheric neutrino flavor ratio R_{ν_μ/ν_e} calculated for several models in comparison with results derived from IceCube experiments [2, 9, 51]. Symbols corresponds to R_{ν_μ/ν_e} reconstructed from the IceCube measurement data, hatched area images these data uncertainties. The filled green area represents R_{ν_μ/ν_e} obtained for sum of the conventional neutrino flux prediction (HGm+QGSJET) and the best-fit astrophysical neutrino flux (Eq. (15)).

ferent pion yield):

$$R_{\nu_\mu/\nu_e}^{(\text{QGSJET})} < R_{\nu_\mu/\nu_e}^{(\text{SIBYLL})} < R_{\nu_\mu/\nu_e}^{(\text{DPMJET})} < R_{\nu_\mu/\nu_e}^{(\text{KM})}.$$

In the range 10 – 100 TeV our calculations with QGSJET-II and SIBYLL give R_{ν_μ/ν_e} values 17 – 25 depending on the cosmic ray spectra (compare ZS+QGSJET-II and HGm+QGSJET-II/SIBYLL, Fig. 7), while the Monte Carlo computation (using the CORSIKA) for same models [33] gives larger values, 25 – 32. The hadronic model by Kimel and Mokhov leads to the neutrino flavor ratio R_{ν_μ/ν_e} rather close to result [56] for DPMJET-III [36, 37] in the range 100 GeV - 10 TeV. In Fig. 7 is seen however, that large values of the flavor ratio like that due to the HGm+KM calculation, $R_{\nu_\mu/\nu_e} \approx 30$ at 10 – 100 TeV, are hardly compatible with the those reconstructed from IceCube data.

Figure 7 shows a rough reconstruction of R_{ν_μ/ν_e} derived from the atmospheric neutrino spectra, measured by IceCube [2, 9]. Diamonds denote R_{ν_μ/ν_e} values reconstructed with usage of the IceCube data [9] and [2], triangles correspond to the latest preliminary IceCube data for the atmospheric electron neutrino spectrum [51]. The hatched area displays the R_{ν_μ/ν_e} statistical uncertainties of the measurement data:

$$\delta R_{\nu_\mu/\nu_e} = R_{\nu_\mu/\nu_e} \sqrt{(\delta\phi_{\nu_\mu}/\phi_{\nu_\mu})^2 + (\delta\phi_{\nu_e}/\phi_{\nu_e})^2}.$$

To derive ν_μ and ν_e flux values at equal energies, a local interpolation of the experimental data is required. This problem was solved by making the interpolating function (a local fit) for the ν_μ spectrum at energies 100 GeV - 20 TeV supported by IceCube40 ν_μ measurement data [2] in the range 141 GeV - 35.5 TeV. As the dominator in the $R_{\nu_\mu/\nu_e}(E)$ ratio taken were exactly experimental values of the IceCube ν_e flux [9] and separately from Ref. [51]. The robustness of the procedure was tested by use, on the contrary, of the ν_μ flux measurement data and a fit for the ν_e spectrum.

The curved band in Fig. 7 is obtained as sum of the calculated conventional neutrino flux (HGm+QGSJET-II, zero prompt neutrino flux) and the astrophysical one in accordance with IceCube best fit [12] (Eq. (15)). To compute $R_{\nu_\mu/\nu_e}(E_\nu)$ in the range below 60 TeV, the IceCube best fit was extrapolated to 10 TeV. No prompt neutrinos were taking into account. The width of the band reflects the IceCube astrophysical flux uncertainty, $\pm 0.3 \cdot 10^{-8} \text{ GeVcm}^{-2}\text{s}^{-1}\text{sr}^{-1}$. The extrapolation of the best-fit astrophysical neutrino flux to the energy range below 60 TeV does not contradicts to R_{ν_μ/ν_e} reconstructed from the IceCube data for atmospheric neutrinos.

The neutrino flavor ratio R_{ν_μ/ν_e} (symbols), extracted from IceCube data, does not reveal a trend to rise that was expected for the conventional neutrino flux in the energy range 100 GeV - 30 TeV (Fig. 7). This behavior probably indicates that the atmospheric electron neutrino flux, obtained in the IceCube experiment, contains an admixture of the astrophysical neutrinos yet in the range 10 - 20 TeV.

In case of zero prompt component, the IceCube best-fit astrophysical neutrino flux dominates over atmospheric ($\nu_e + \bar{\nu}_e$) flux at energies above 50 TeV. Close to 50 TeV the predicted (HGm+QGSJET) atmospheric conventional ν_e flux (scaled by E^{-2}) is about $0.46 \cdot 10^{-8} \text{ GeVcm}^{-2}\text{s}^{-1}\text{sr}^{-1}$, that is less by half of the best-fit astrophysical flux. Alternative hypothesis, allowing for the prompt neutrino component, which leads to similar depression of R_{ν_μ/ν_e} , also might be accepted, but the the prompt neutrino flux in this case should be rather large one, like the QGSM predictions.

V. SUMMARY

The problem of the atmospheric neutrino background became really important after observation with the IceCube detector of events induced by very high-energy neutrinos of extraterrestrial origin [10-12]. More precise calculations of the high-energy neutrino spectrum are required because neutrino fluxes from astrophysical sources are probably entangled with atmospheric fluxes of neutrino arising from decays of π , K mesons (conventional neutrinos) and charmed particles (prompt neutrinos) which are produced in collisions of cosmic ray particles with atomic nuclei of the Earth's atmosphere.

In this work we present the results of the calculations of the high-energy atmospheric neutrino fluxes performed for hadronic interaction models QGSJET-II-03, SIBYLL 2.1 and Kimel & Mokhov, taking into consideration the “knee” of the cosmic-ray spectrum. The calculation revealed rather weak dependence on the cosmic ray spectrum in the energy range $10^2 - 10^5$ GeV. However the picture appears to be less steady because of sizable difference of the hadronic models predictions. As it can be seen by the example of the models QGSJET II-03 and SIBYLL 2.1, the major factor of the discrepancy in conventional neutrino fluxes is the kaon production in nucleon-nucleus collisions. Really, cosmic-ray physicists feel necessity of comprehensive analysis of the actual features of the high-energy hadronic models under discussion, QGSJET II-03 (04), EPOS-LHC, SIBYLL 2.1, DPMJET-III, especially concerning details of the kaon and charmed particle production in NA -, πA -collisions.

Above 100 TeV calculated spectra of muon neutrinos display the apparent dependence on the spectrum and composition of primary cosmic rays related to the “knee” range. Also in this region uncertainties appear due to production cross sections and decays of charmed particles which imprint on the prompt neutrino flux.

All calculations are compared with the atmospheric neutrino measurements by Frejus, AMANDA, IceCube and ANTARES. New reconstruction of the ν_μ spectrum, performed by IceCube Collaboration [46], give support for the QGSM prompt neutrino flux prediction. Being in a close agreement with the IceCube measurement data in the energy range from 140 GeV to 100 TeV, the HGm+QGSJET model leads to the systematic deviation from experimental data, especially those for the IceCube59 muon neutrino spectrum in energy the range 100 - 500 TeV. Thus the IceCube59 data leaves a window for the QGSM prompt neutrino component: the comparison of the calculation with IceCube measurement data on atmospheric ν_μ and ν_e fluxes makes possible to consider the HGm+QGSJET-II-03+QGSM model as the preferable one.

The approximation formula describing the HGm+QGSJET-II-03 predictions of the atmospheric conventional $\nu_e + \bar{\nu}_e$ and $(\nu_\mu + \bar{\nu}_\mu)$ energy spectra, averaged over zenith angles, is given by Eq. (14). An analytic description of $\nu_\mu + \bar{\nu}_\mu$ and $\nu_e + \bar{\nu}_e$ energy spectra HGm+QGSJET-II-03 can be used, in principle, as one more tool to test data of neutrino event reconstruction in neutrino telescopes.

Authors of the IceCube59 analysis [46] avoid definite conclusions concerning the prompt neutrino contribution or the neutrinos of a cosmic origin because of large systematic uncertainties at the highest energies. Nevertheless the ν_μ flux mean values illustrate the state of the problem. Even if the prompt neutrino flux is zero, sum of the best-fit astrophysical flux and the calculated atmospheric conventional one, gives the evidently higher flux as compared to the IceCube59 data (the last bin around $E_\nu \approx 575$ TeV). This circumstance gives rise to doubts

regarding the hypothesis of equal flavor composition the IceCube astrophysical flux, $\nu_e : \nu_\mu : \nu_\tau = 1 : 1 : 1$.

The IceCube best-fit astrophysical neutrino flux dominates over atmospheric ($\nu_e + \bar{\nu}_e$) flux at energies above 60 TeV (Fig. 6). At 60 TeV the highest predicted (HGM+SIBYLL) atmospheric conventional ν_e flux (scaled by E^{-2}) is about $0.5 \cdot 10^{-8} \text{ GeV cm}^{-2} \text{ s}^{-1} \text{ sr}^{-1}$, that is below the IceCube best-fit astrophysical flux, Eq. (15). Thus the transition from the atmospheric electron neutrino flux to the predominance of the astrophysical neutrinos occurs probably at 30 – 100 TeV, if the prompt neutrino component is taken into consideration.

The Kimel & Mokhov hadronic model (HGM+KM) as well as DPMJET-III [56] leads to the atmospheric neutrino flavor ratio, R_{ν_μ/ν_e} , similar to that obtained in the MC computation [33] ($R_{\nu_\mu/\nu_e} \approx 25 - 32$ at $E_\nu = 10 - 100$ TeV) for QGSJET-II and SIBYLL 2.1 models, which is hardly compatible with R_{ν_μ/ν_e} reconstructed from IceCube data.

If the power law E^{-2} is valid for the astrophysical neutrino spectrum at energies below 60 TeV then extrapolation to lower energies of the high-energy neutrino flux, observed in the IceCube experiment [10–12], should lead to decrease of the neutrino flavor ratio R_{ν_μ/ν_e} in the energy range 10 – 50. This extrapolation shows the consistency of the ratio R_{ν_μ/ν_e} , calculated with model HGM+QGSJET-II-03, and that of obtained from the IceCube data. The computation of neutrino flavor ratio hints that one more confirmation of astrophysical origin for high-energy neutrino events might be obtained from

little progress in measurement of the ν_e spectrum above 20 TeV, because R_{ν_μ/ν_e} , more sensitive to the electron neutrino flux, allows to reveal a small fraction from astrophysical sources.

The neutrino flavor ratio R_{ν_μ/ν_e} , extracted from IceCube data, does not reveal a trend to rise as it is expected for the conventional neutrino flux in the energy range 100 GeV – 30 TeV (Fig. 7). The explanation of this apparent tendency can be connected with the astrophysical neutrinos appeared exactly against the atmospheric electron neutrino flux at rather low energies around 10 – 20 TeV. Thus the depression of the ratio R_{ν_μ/ν_e} probably serves as an indication that the atmospheric electron neutrino flux measured in the IceCube experiment contains the admixture of the astrophysical neutrinos in the energy range 10 – 50 TeV.

ACKNOWLEDGMENTS

We thank V. A. Naumov for helpful discussions and comments. Authors are grateful to A. A. Kochanov for considerable assistance in computations.

We acknowledge the support from the Russian Federation Ministry of education and science (the agreement 14.B37.21.0785, zadanie 3.889.2014/K) and the Russian Foundation for Basic Research, grant 13-02-00214. The research was supported in part also by the grant of President of Russian Federation NSh-3003-2014-2.

-
- [1] V. Aynutdinov et al., Nucl. Instrum. Meth. A **588**, 99 (2008).
 - [2] R. Abbasi et al. (IceCube Collaboration), Phys. Rev. D **83**, 012001 (2011).
 - [3] R. Abbasi et al. (IceCube Collaboration), Phys. Rev. D **84** (2011) 082001.
 - [4] R. Abbasi et al. (IceCube Collaboration), Phys. Rev. D **83**, 092003 (2011).
 - [5] S. Adrian-Martinez et al. Eur. Phys. J. C **73**, 2606 (2013).
 - [6] V. Van Elewyck (ANTARES Collaboration), Nucl. Instrum. Meth. A **742**, 63 (2014).
 - [7] K. Daum et al., Z. Phys. C **66**, 417 (1995).
 - [8] R. Abbasi et al. (IceCube Collaboration), Astropart. Phys. **34**, 48 (2010).
 - [9] M. G. Aartsen et al. (IceCube Collaboration), Phys. Rev. Lett. **110**, 151105 (2013); arXiv:1212.4760v1.
 - [10] M. G. Aartsen et al. (IceCube Collaboration), Phys. Rev. Lett. **111**, 021103 (2013).
 - [11] M. G. Aartsen et al. (IceCube Collaboration), Science **342**, 1242856 (2013);
 - [12] M. G. Aartsen et al. (IceCube Collaboration), Phys. Rev. Lett. **113**, 101101 (2014); arXiv:1405.5303v2.
 - [13] K. Murase, M. Ahlers, B.C. Lacki, Phys. Rev. D **88**, 121301(R) (2013); arXiv:1306.3417.
 - [14] Ranjan Laha et al., Phys. Rev. D **88**, 043009 (2013); arXiv:1306.2309.
 - [15] F. W. Stecker, Phys. Rev. D **88**, 047301 (2013)
 - [16] S. Ostapchenko, Phys. Rev. D **74**, 014026 (2006); Nucl. Phys. B (Proc. Suppl.) **175-176**, 73 (2008); ibid. **151**, 143 (2006).
 - [17] E.J. Ahn, R. Engel, T. K. Gaisser, P. Lipari, T. Stanev Phys. Rev. D **80**, 094003 (2009). R.S. Fletcher et al. Phys. Rev. D **50**, 5710 (1994).
 - [18] A.A. Kochanov, T.S. Sinogovskaya, S.I. Sinogovskiy, Astropart. Phys. **30**, 219 (2008).
 - [19] A.A. Kochanov, T.S. Sinogovskaya, S.I. Sinogovskiy, J. Exp. Theor. Phys. **116**, 395 (2013); Zh. Eksp. Teor. Fiz. **143**, 459 (2013).
 - [20] A.N. Kalinovsky, N.V. Mokhov, Yu.P. Nikitin, 1989. Passage of high-energy particles through matter, New York, USA: AIP (1989) 262 p.
 - [21] V.I. Zatsepin, N.V. Sokolskaya, Astronomy & Astrophys. **458**, 1 (2006).
 - [22] A. M. Hillas, arXiv:astro-ph/0607109v2.
 - [23] T. K. Gaisser, Astropart. Phys. **35**, 801 (2012);
 - [24] D. Bindig, C. Bleve, K.-H. Kampert, in Proc. of 32nd ICRC, Beijing, 2011, Vol. 1, p. 161.
 - [25] J. Horandel, Astropart. Phys. **19**, 193 (2003); **21**, 241 (2004).
 - [26] V. A. Naumov, T. S. Sinogovskaya, Phys. Atom. Nucl. **63**, 1927 (2000); hep-ph/0106015.
 - [27] S.I. Sinogovskiy et al. Int. J. Mod. Phys. A **25**, 3733

- (2010); arXiv:0906.3791.
- [28] A.C. Genz, A.A. Malik, *J. Comput. Appl. Math.* **6**, 295 (1980).
- [29] T. Antoni et al., *Astropart. Phys.* **24**, 1 (2005).
- [30] A.D. Panov et al., *Bull.Russ. Acad. Sci.Phys.* **71**, 494 (2007); *ibid.* **73**, 564 (2009).
- [31] H.S. Ahn et al., *Ap. J. Lett.* **714**, L89 (2010); H.S. Ahn et al., *Ap. J.* **707**, 593 (2009).
- [32] M. G. Aartsen et al. (IceCube Collaboration), *Phys.Rev. D* **89**, 062007 (2014); arXiv:1311.7048.
- [33] A. Fedynitch, J. Becker Tjus, P. Desiati, *Phys. Rev. D* **86**, 114024 (2012).
- [34] G. Fiorentini, V. A. Naumov, F. L. Villante, *Phys. Lett. B* **510**, 173 (2001).
- [35] V.A. Naumov, In the Proceedings of the 2nd Workshop on Methodical Aspects of Underwater/Underice Neutrino Telescopes, Ed. by R. Wischniewski (DESY, Hamburg, 2002); hep-ph/0201310v2.
- [36] S. Roesler, R. Engel, J. Ranft, hep-ph/0012252.
- [37] T. Sanuki, M. Honda, T. Kajita, K. Kasahara, S. Midorikawa, *Phys. Rev. D* **75**, 043005 (2007).
- [38] L. Derome, *Phys. Rev. D* **74**, 105002 (2006).
- [39] T.K. Gaisser, M. Honda, *Annu. Rev. Nucl. Part. Sci.* **52**, 153 (2002).
- [40] S.I. Sinigovsky, O.N. Petrova, T.S. Sinigovskaya, in Proceedings of 32nd International Cosmic Ray Conference, Beijing, 2011, ed. Hongbo Hu (Institute of High Energy Physics, Beijing, 2011), Vol. 4, p. 291; arXiv:1109.3576.
- [41] O. N. Petrova, T. S. Sinigovskaya, S. I. Sinigovsky, *Phys. Part. Nucl. Lett.* **9**, 766 (2012).
- [42] S. I. Sinigovsky, E. V. Ogorodnikova, T. S. Sinigovskaya, 33d International Cosmic Ray Conference, Rio de Janeiro, 2013; arXiv:1306.5907v2.
- [43] A. B. Kaidalov, O. I. Piskunova, *Sov. J. Nucl. Phys.* **41**, 816 (1985); *Sov. J. Nucl. Phys.* **43**, 994 (1986); *Z. Phys. C* **30**, 145 (1986).
- [44] E. V. Bugaev et al. *Nuovo Cim. C* **12**, 41 (1989).
- [45] S. I. Nikolsky, I. N. Stamenov, S. Z. Ushev, *Zh. Eksp. Teor. Fiz.* **87**, 18 (1984) [*Sov. Phys. JETP* **60**, 10 (1984)].
- [46] M. G. Aartsen et al. (IceCube Collaboration), arXiv:1409.4535v2 [astro-ph.HE] (2014)
- [47] O. Mena, S. Palomares-Ruiz, A. C. Vincent, *Phys. Rev. Lett.* **113**, 091103 (2014).
- [48] R. Enberg, M.H. Reno, I. Sarcevic, *Phys. Rev. D* **78**, 043005 (2008).
- [49] It should be noted that the contribution of semileptonic decay $K_S^0 \rightarrow \pi e \nu_e$ into the atmospheric ν_e flux was taking into account long ago [35], contrary to the assertion in Ref. [50]: “We have identified a hitherto overlooked contribution to the conventional atmospheric ν_e flux, from $K_S \rightarrow \pi e \nu_e$.” Since 1999 calculations of the atmospheric electron neutrino flux included this source by default after T. Sinigovskaya, PhD thesis (Irkutsk State University, 1999) and V. Naumov [35]. The citation from Ref. [35] (p. 12): “The high-energy calculation takes into account many thin effects, like K_{e3} and $K_{\mu 3}$ form factors and K_S^0 semileptonic decays, meson regeneration and charge exchange through reactions $\pi^\pm + \text{Air} \rightarrow \pi^\pm(\mp) + X$, $\pi^\pm + \text{Air} \rightarrow K^\pm(0) + X$, etc., as well as through $K_{\pi 2}$ and $K_{\pi 3}$ decays.” The latest calculations of atmospheric ν_e flux [40–42] included also the K_S^0 semileptonic decay.
- [50] T.K. Gaisser, S.R. Klein, arXiv:1409.4924v1.
- [51] G. Binder, Probing the Transition from Atmospheric to Astrophysical Neutrinos in IceCube. Talk given at 18th ISVHECRI 18-22 Aug. 2014, CERN, Geneva (unpublished), <https://indico.cern.ch/event/287474/other-view?view=standard>
- [52] D. Fargion, P. Paggi, arXiv:1310.3543v4.
- [53] Lingjun Fu, Chiu Man Ho, arXiv:1407.1090v2.
- [54] Xun-Jie Xu, Hong-Jian He, Werner Rodejohann, arXiv:1407.3736v2.
- [55] Chien-Yi Chen, P. S. Bhupal Dev, Amarjit Soni, arXiv:1411.5658v2.
- [56] M. Honda, T. Kajita, K. Kasahara, S. Midorikawa, T. Sanuki, *Phys. Rev. D* **75**, 043006 (2007).